Histol Histopathol (2007) 22: 261-272

http://www.hh.um.es

Histology and Histopathology

Cellular and Molecular Biology

Ultrastructural characterization of calcification onset and progression in subdermally implanted aortic valves. Histochemical and spectrometric data

F. Ortolani[1,2], A. Bonetti[1], F. Tubaro[3], L. Petrelli[1], M. Contin[1], S.L. Nori[4], M. Spina[5] and M. Marchini[1,2]

[1]Department of Medical Morphological Research, University of Udine, Udine, Italy,

[2]Interdepartmental Center for Regenerative Medicine (C.I.M.E.), University of Udine, Udine, Italy,

[3]Department of Chemical Sciences and Technology, University of Udine, Udine, Italy, [4]Institute of Human Anatomy, Catholic University, Rome, Italy and [5]Department of Experimental Biomedical Sciences, University of Padua, Padua, Italy

Summary. Detailed characterization of the subdermal model is a significant tool for better understanding of calcification mechanisms occurring in heart valves. In previous ultrastructural investigation on six-week-implantated aortic valve leaflets, modified pre-embedding glutaraldehyde-cuprolinic-blue reactions (GA-CB) enabled sample decalcification with concurrent retention/staining of lipid-containing polyanionic material, which lined cells and cell-derived matrix-vesicle-like bodies (phthalocyanin-positive layers: PPLs) co-localizing with the earliest apatite nucleation sites. Additional post-embedding silver staining (GA-CB-S) revealed PPLs to contain calcium-binding sites. This investigation concerns valve leaflets subjected to shorter implantation times to shed light on the modifications associated with PPLs generation and calcification onset/progression. Spectrometric estimations revealed time-dependent calcium increase, for unreacted samples, and copper modifications indicating an increase in acidic, non-glycanic material, for GA-CB-reacted samples. Two-day-implant thin sections showed emission and subsequent reabsorption of lamellipodium-like protrusions by cells, originating ECM-containing vacuoles, and/or degeneration stages characterized by the appearance of GA-CB-S-reactive, organule-derived dense bodies and progressive dissolution of all cell membranes. In one-week-implants, the first PPL-lined cells were found to co-exist with cells where GA-CB-S-reactive material accumulated, or exudated towards their edges, or outcropped at the ECM milieu, so acquiring PPL features. PPL-derived material was observed increasingly to affect the ECM on thin sections of one-week- to six-week-implants. These results show an endogenous source for PPLs and reveal that a peculiar cascade of cell degenerative steps is associated with valve mineralization in the subdermal model, providing new useful parameters for more reliable comparison of this experimental calcification process *versus* the physiological and pathological processes.

Key words: Aortic valve calcification, Ultrastructural cell degeneration, Subdermal model, Cuprolinic blue, von Kossa

Offprint requests to: Dr. F. Ortolani, Department of Medical Morphological Research, University of Udine, Piazzale Kolbe 3, I-33100, Udine, Italy. e-mail: fulvia.ortolani@uniud.it

Introduction

Detailed characterization of any animal model is a significant tool for both biological and clinical purposes because it provides clues for (i) better understanding of the mechanisms occurring in various calcification processes; (ii) more reliable screening of anti-mineralization properties of existing heart bioprosthetic valves; and (iii) more appropriate design of novel bioprostheses.

The subcutaneous implant model is the most widely used experimental approach for predicting post-operative susceptibility to calcification of heart bioprosthetic valves because of their relatively low cost and the precocity of mineralization onset, which starts within a few hours, and accelerated mineralization, which terminates within 8 weeks (Schoen et al., 1985; Mako and Vesely, 1997). In addition, structural changes were found to closely mimic those in circulatory models or in surgical explants (Schoen et al., 1985, 1992). These findings are consistent with the accepted concept that calcification generally occurs according to common

patterns (Fishbein et al., 1982; Anderson, 1983; Bonucci, 1984; Boskey et al., 1988). However, it has also been claimed that distinct differences exist among different types of mineralization, for example dystrophic *versus* physiological calcification (Nimni et al., 1988), or bioprosthetic valve calcification *versus* native (Chanda et al., 1997).

Additional insights concerning the involvement of specific molecules, such as proteoglycans and lipids (Jorge-Herrero et al., 1991), alkaline phosphatase (Maranto and Schoen, 1988; Levy et al., 1991), osteocalcin (Levy et al., 1980, 1983), or osteopontin (Shen et al., 1997; Srivatsa et al., 1997) in valve mineralization, support the idea that at least some features are shared by all calcification types.

Investigations into tissue changes during calcification onset and progression in subdermally implanted porcine aortic valve leaflets (Schoen et al., 1985) and pericardium-derived valve bioprostheses (Schoen et al., 1986) have supplied additional information on the mechanisms underlying this mineralization process: cell plasmalemmas, cell-derived matrix-vesicle-like bodies, mitochondria and nuclei have been identified as major apatite crystal nucleators, with collagen fibrils possibly acting as minor ones.

Further ultrastructural insights have been acquired into the valve calcification process in heterologous subdermal environments using modified histochemical procedures involving sample unmasking from mineral with associated retention and visualization of polyanionic lipid material (Ortolani et al., 2002a,b, 2003). Namely, (i) modified pre-embedding reactions with copper phthalocyanin Cuprolinic Blue (GA-CB) revealed peculiar electron-dense layers (Phthalocyanin Positive Layers: PPLs) lining cells and cell-derived matrix-vesicle-like bodies, co-localising with the earlier sites of apatite crystal nucleation; (ii) additional post-embedding von Kossa silver staining (GA-CB-S) applied to electron microscopy showed PPLs to be rich in calcium-binding sites; and (iii) modified reactions with Malachite Green showed PPLs also to contain acidic phospholipid moieties. In addition, PPL-like material was observed to spread outside mineralized cells triggering ECM calcification.

The above results were observed for 6-week-long subdermal implantations only. It was not possible to assess all the upstream tissue modifications or to understand whether PPL formation should be ascribed to endogenous or exogenous phenomena. In the present investigation, the above modified histochemical procedure and spectrometric analyses were extended to porcine aortic valve leaflets retrieved from rat subcutis after different implantation times. The aim was to assess (i) how cell degeneration starts; (ii) how it correlates with early calcification; (iii) and how PPLs generate.

Spectrometric analyses showed a time-dependent increase of calcium amounts and peculiar changes in copper amounts, indicating that actually non-glycanic polyanion accumulation is associated with calcific progression in the subdermal model. In addition, ultrastructural analysis revealed specific time-related changes including increasing release and clustering within cells of GA-CB-S-reactive material which proved to represent an endogenous PPL-source, because of subsequent layering and outcropping at cell surfaces.

Material and methods

Subcutaneous implant model

Fifteen aortic roots were dissected from adult pigs (n=15; mean age and weight were 18 weeks and 80 kg, respectively) and subjected to experimental calcification (Schoen et al. 1986). The samples were suspended in 0.625% (w/v) glutaraldehyde (Fluka, BioChemika) in degassed and continuously stirred 10 mM borate buffer, pH 7.4, containing 0.9% (w/v) NaCl, in the dark and under N_2 atmosphere. After 6 h, the aortic roots were re-suspended in fresh solution, treated in the same conditions for a further 16 h, and then stored in 0.2% (w/v) glutaraldehyde in borate buffer for 2 days. Fifteen aortic valve leaflets, dissected from the above aortic roots (1 leaflet per root) and subdermally implanted into abdominal pouches obtained in 3-week-old male Sprague-Dawley rats (1 leaflet per rat) for 2 days, 1 week, 2 weeks, 4 weeks or 6 weeks (n=3 for implantation time). After retrieval, the valve leaflets were washed for 1 min, once in 0.9% (w/v)NaCl and twice in deionized water, and then freeze-dried.

Sampling

After rehydration of the valve leaflets with 10mM borate buffer, pH 7.4, containing 0.9% (w/v) NaCl, samples were excised and grouped into 3 lots for light microscopy, electron microscopy and mass spectrometry, respectively. Control samples were excised from unimplanted valve leaflets. The samples were sized to about 8 mm x 2 mm for the first lot, to about 1 mm x 1mm for the second lot, or reduced to 2±0.2 mg in weight for the third lot.

Light microscopy

Samples from lot 1 plus control samples were dehydrated in graded ethanols and embedded in paraffin. Histological sections underwent von Kossa silver staining and were mounted on glass slides. Subsequently, the sections underwent incubation in 1% $AgNO_3$ aqueous solution at room temperature with exposure to sunlight for 15 min; washing in distilled water and drying; and reduction with 5% sodium thiosulphate in aqueous solution for 5 min at room temperature.

Electron microscopy

Samples from lot 2 plus control samples were

processed for both conventional visualization and histochemical localization of polyanions and Ca-binding sites.

Conventional processing

Samples underwent fixation with 2.5% glutaraldehyde in 0.1M phosphate buffer, pH 7.4; post-fixation with 2% OsO_4 dissolved in buffer as above; dehydration in graded ethanols; and embedding in Araldite/Epon.

Histochemical processing for polyanion localization (GA-CB reaction)

Samples were washed in 25 mM sodium acetate solution containing 0.05M $MgCl_2$, pH 4.8, for 1 h; fixed/reacted with 2.5% glutaraldehyde (GA) and 0.05% Cuprolinic Blue (CB) (Electron Microscopy Science) in acetate buffer as above, overnight, using an Agar specimen rotator; washed twice in acetate buffer as above; washed in 0.1M phosphate buffer, pH 7.2; and post-fixed with 2% OsO_4 dissolved in 0.1M phosphate buffer as above, for 1h. The GA-CB-reacted samples were then post-fixed and embedded with conventional procedure as above.

Histochemical processing for the localization of Ca-binding sites (GA-CB-S reaction)

Semi-thin sections from samples of lot 2 (GA-CB-reacted sections) were subjected to post-embedding von Kossa silver staining as for the histological sections, except for incubation and reduction phase temperature, which was set at 80°C by placing the glass slides on warm plates. Ultrathin sections were taken from these GA-CB-S-reacted semi-thin sections once re-embedded. Namely, after top cutting, conic Beem capsules (Agar Scientific) were (i) cut at the top, (ii) placed onto slides encircling single mounted semi-thin sections, (iii) glued at their bases, (iv) and filled with epon-araldite fluid. After resin-polymerization, these new inclusions were detached from the slides after freezing at -80°C and subjected to ultramicrotomy.

Staining and recording

All ultrathin sections were placed on formvar-coated copper grids, Slot 2x1, and contrasted with uranyl acetate and lead citrate. Observations and micrographic records were made using a Philips CM12 transmission electron microscope.

Mass spectrometry

Samples from lot 3 plus control samples were subjected to GA-CB-reactions (i) at 0.05M $MgCl_2$ CEC conditions, as for lot 2 samples, and (ii) 0.3M $MgCl_2$ CEC conditions. After the GA-CB-reactions, the samples were solubilized by digestion with 50µL of concentrated HNO_3 (65%), at 50°C for 10 min. The resulting solutions were diluted to 1 mL with ultrapure water.

For ICP-MS analyses, all chemicals used were of analytical reagent-grade quality and were used as received. Stock standard solutions of both Ca and Cu for ICP analyses were obtained by diluting as required the corresponding 1000 mg/L standard solution for ICP (Merck) with ultrapure water, purified with an Elgastat UHQ-PS system, in all cases with the addition of 0.5 % ultrapure-grade 65% HNO_3 (Merck Suprapur). All spectrometric measurements were performed using a Spectromass 2000 Type MSDIA10B (Spectro Analytical Instruments, D). The working frequency was 27.12 MHz with an RF power of 1350 W. Pure argon (transistor quality) was used for all measurements. Measurements were performed after calibrating the gas flows and the plasma position with respect to the interface and the ion-optical parameters to maximize the signal over background noise for both analytes investigated. Optimization was achieved by using the two 1000 mg/L standard solutions, prepared as described above, containing calcium and copper, respectively. All analytical data were collected under standard laboratory conditions, i.e., not in a clean-room environment. Calcium isotope 44 and copper isotope 65 were used. Results were the mean of 10 measurements.

Results

Spectrometric estimations of Ca content in samples from explanted valve leaflets revealed that mineralization had already started in 2-day implants and increased progressively with time, rising tenfold in 6-week implants versus 2-day-ones (Fig. 1). In control samples from unimplanted valve leaflets, only negligible traces of Ca were detected.

Since histochemical CB-reactions used for ultrastructural analysis do not provide quantitative outcomes, and CB is a copper-phthalocyanin, spectrometric estimations of Cu retained by explants previously subjected to GA-CB-reaction and washing were carried out to gain quantitative information on reaction rates (Fig. 2). As expected, lower quantities of Cu were detected in unimplanted samples after reactions performed at 0.3M CEC conditions than at 0.05M. After reactions at 0.3M CEC conditions, amounts of Cu retained fell progressively according to implantation times up to 2 weeks, with an almost 70% decrease, tending to plateau for the two longer implantation times. After reactions performed at 0.05M CEC conditions, Cu content diminished up to 2 weeks as for 0.3M CEC conditions, but at a slower rate, falling by about 30% versus 70%. Moreover, a reverse trend was observed for longer implantation times, with a slight increase of about 7% between 2 and 4-week implantation times, and an increase of about 15% between 2 and 6 weeks.

After von Kossa staining, histological sections (not

shown) supported previous reports concerning subcutaneously implanted aortic valve leaflets (Ferrans et al., 1980; Levy et al., 1983; Schoen et al., 1985; Ortolani et al., 2002a), including the appearance of first mineralization within the intermediate layer, the tunica spongiosa, as well as more advanced progression of the process in this layer *versus* the two surfacing layers, the *tunica ventricularis* and *tunica fibrosa*.

For concision, the following observations will be restricted to this intermediate layer.

On histological sections (not shown), 2-day-implants showed diffuse silver precipitation on the body of many cells and complete unreactivity for the ECM. In 1-week-implants, the great majority of cells proved to be reactive, with several being weakly stained at the cores and markedly stained at the edges. This latter reactivity pattern became prevalent in sections from 2-week-implants, where initial silver precipitation also involved juxtacellular ECM. On sections of 4-week- and 6-week-implants, increased silver precipitation was observed in ECM, revealing the presence of increasingly numerous, broad calcific foci.

After traditional processing (not shown), thin sections of 2-day-implants revealed initial calcification consisting of amorphous calcium deposition on most interstitial cells, with marked masking effects. Some apatite crystal was occasionally found on cell surfaces or at mitochondrion level. Increased mineralization in 1-week-implants was revealed by amorphous calcium deposition affecting all cells, as well as initial precipitation of apatite crystals around several cells. On thin sections of 2-week-implants, prominent precipitation of apatite crystals was present at the edges of most cells, also involving juxtacellular ECM. Further crystal precipitation in ECM was observed on thin sections of 4-week- and 6-week-implants because of increasingly numerous, extensive calcific foci.

Owing to concurrent decalcification effect, pre-embedding CB-reactions clearly revealed a specific repertoire of cell features on 2-day-implant thin sections. These observations were (i) the presence of many convoluted lamellipodium-like cytoplasmic protrusions; (ii) heterogeneous cytoplasm vacuolization; (iii) the appearance of seemingly lysosome-derived dense bodies; (iv) scarcity of ribosomes, and (v) weakening and/or initial dissolution of plasmalemmas, nuclear envelopes and organule membranes (Fig. 3A-F). Cytomembrane dissolution and a concurrent increase in electron-density of adjacent material led to their appearance as electron-lucent linear profiles against a dark background (Fig. 3B,C). The occasional presence of crista-derived cross striations enabled prompt identification of degenerating mitochondria among the organules involved in dense body generation. The largest heterogeneous vacuoles clearly appeared to result from secondary self-merging of adjacent cytoplasmic lamellae (Fig. 3D) or the merging of their free edges with the cell body (Fig. 3E). These phagosome-like vacuoles therefore contained ECM-derived particles (Figs. 3C-F). Confluencing of these large vacuoles and dense bodies was also often apparent (Fig. 3C-F). More advanced alteration stages were represented by: (i) cell outlines acquiring blunt features (Fig. 3F,G) because of complete re-absorption of lamellipodia; (ii) overall membrane dissolution; and (iii) increasing cytoplasm electron-density, spanning the entire cytoplasm (Fig. 3G). The accumulating osmiophylic, CB-reactive material which caused the increase in cytoplasm electron-density is here

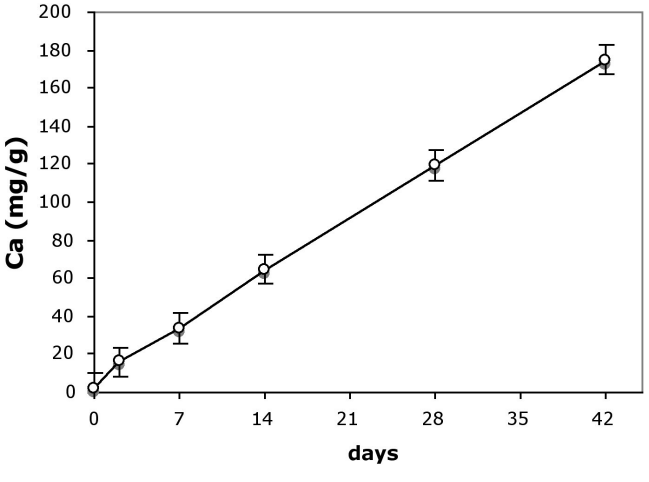

Fig. 1. Total amount of Ca estimated after digestion with HNO_3 of aortic valve leaflets subdermally implanted for 2 day- to 6 week-long times.

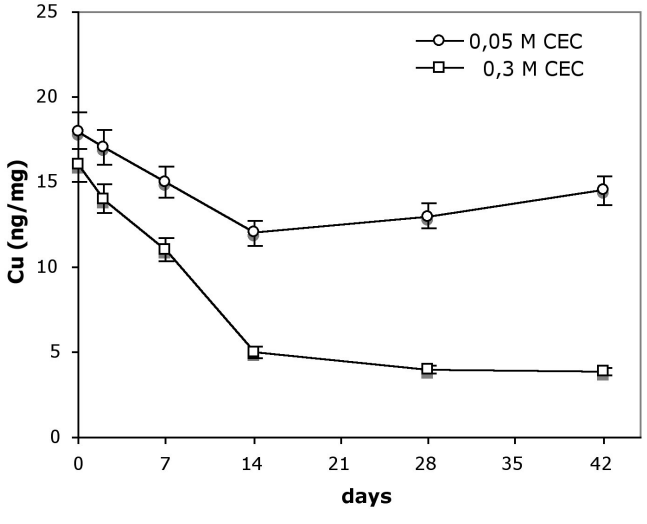

Fig. 2. Total amount of Cu estimated after digestion with HNO_3 of aortic valve leaflets subdermally implanted for 2 day- to 6 week-long times and then subjected to GA-CB-reactions at 0.05M and 0.3M CEC conditions.

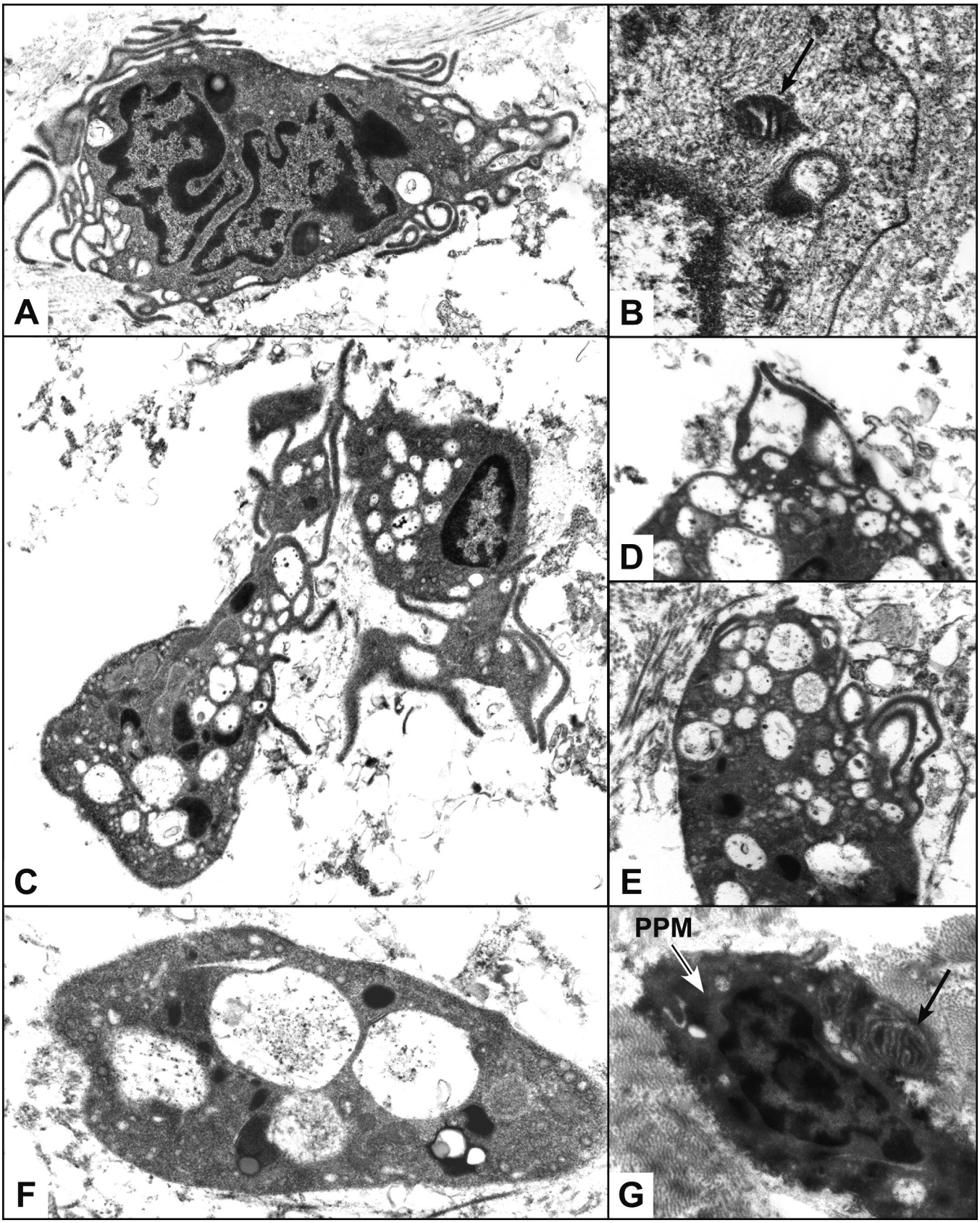

Fig. 3. *Tunica spongiosa* of porcine aortic valve leaflet implanted in rat sub-cutis for 2 days. **A, C-E**. Presence of lamellipode-like extrusions. **A, G.** Presence of dense bodies. **B.** CB-reactivity associated with organule degeneration: a degenerating mitochondrion is recognizable (arrow). **C-G**. Cytoplasm vacuolization and cytomembrane disappearance. **G.** A Cytoplasm filled with GB-reactive material (PPM) is indicated by a black-and-white arrow; a black arrow points electronlucent profiles subsequent to plasmalemma dissolution after lamellipodium twining and re-compactation. A, x 10,500; B, x 38,000; C, x 10,000; D, E, x 12,000; F, x 19,000; G, x 9,500

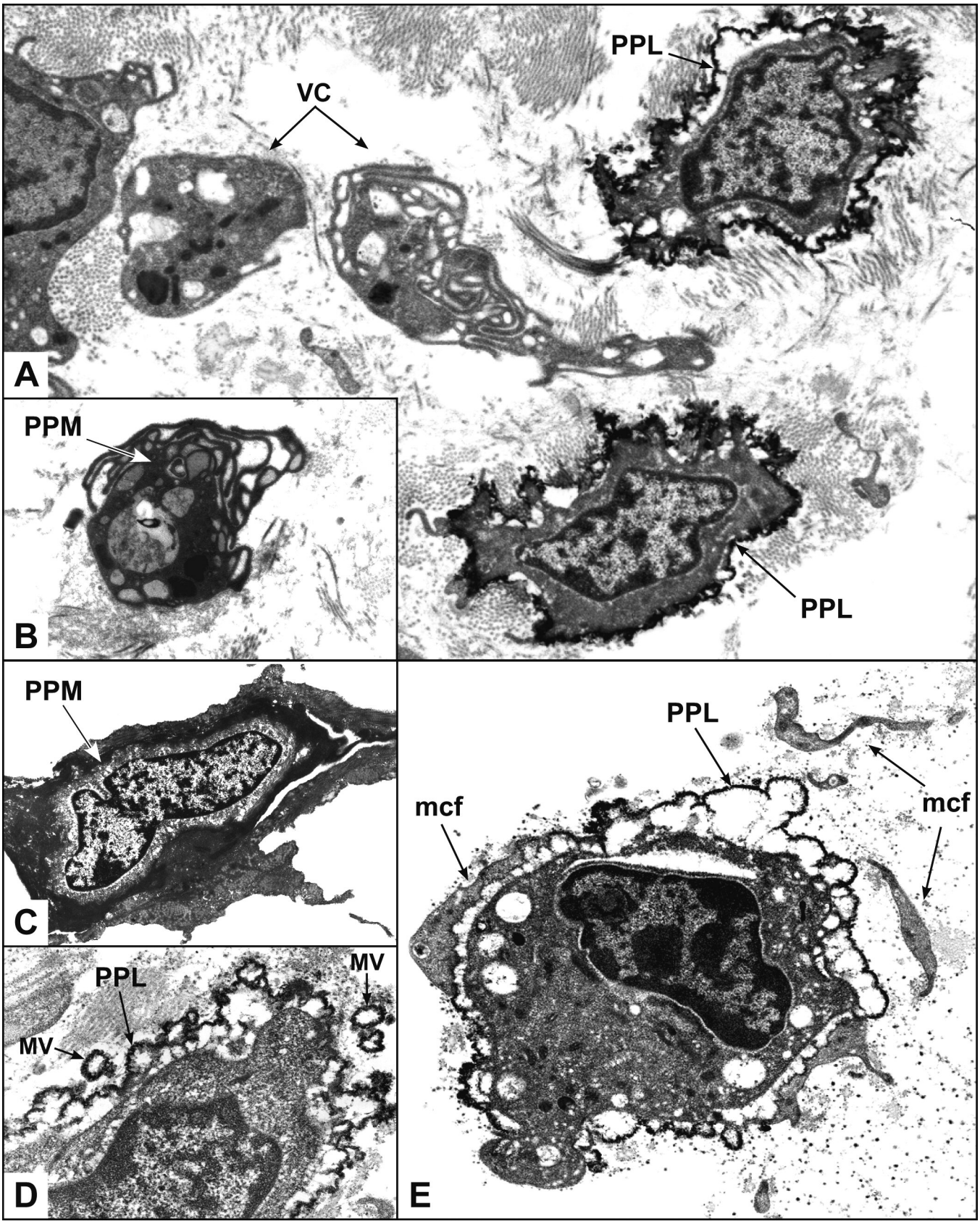

Fig. 4. *Tunica spongiosa* of porcine aortic valve leaflet implanted in rat sub-cutis for 1 week. **A.** Co-presence of vacuolated cells (VC) and cells lined by phthalocyanine-positive-layers (PPL). **B.** Presence of diffuse PPM within vacuolated cells. **C.** Moving of PPM towards cortical cytoplasm. **A, D, E.** Presence of PPLs. **D.** Budding of matrix-vesicle-like bodies (MV). **E.** precocious PPL generation with associated detaching of marginal cytoplasm fragments (mcf). A, x 12,000; B, x 8,000; C, x 6,000; D, x 17,000; E, x 11,000

referred to as PPM (phthalocyanin-positive material).

On thin sections of CB-reacted 1-week-implants, the cells exhibited further features suggesting ongoing serial changes, with the two end-points represented by vacuolated cells, as for 2-day-implants, and still rare cells which were lined by 40 to 60 nm-thick electron-dense layers (Fig. 4A). These pericellular layers were identical to the phthalocyanin-positive layers already described for 6-week-implant cells and named PPLs (Ortolani et al., 2002a), as in the current work. Transitional features were represented by cells exhibiting diffuse PPM in cytoplasms (Fig. 4B) and cells where the original electron-transparency was being recovered in the inner cytoplasm while electron-density was increasing in the cortical cytoplasm (Fig. 4C). Within the cleaned cytoplasms, the (i) absence of ribosomes; (ii) sporadic presence of membrane-deprived organule ghosts; and (iii) permanence of the cytoskeleton network were observed.

Collectively, the stages observed indicated that PPM was first released filling the whole cytoplasm, and then moved centrifugally to condensate at cell edges so forming PPLs, which gave rise to initial blebbing of cytoplasm-lacking matrix vesicle-like bodies (Fig. 4D). PPM did not reach the cell surface as a rule, because premature condensation into PPL was sometimes occurring within the cortical cytoplasm; subsequent detachment of marginal cytoplasm fragments in any case entailed secondary PPL exposure to the ECM (Fig. 4E).

Thin sections of CB-reacted 2-week-implants showed most cells exhibiting PPLs, which topically seemed to spread outwards embedding electron-lucent collagen fibrils (Fig. 5A) and elastin fibers (Fig. 5B).

No further degenerative features were observed on thin sections of 4-week- and 6-week-implants, the only apparent difference being an increasingly marked spreading of CB-reactive material into the ECM.

Post-embedding von Kossa reactions performed on semi-thin sections of CB-reacted implants entailed selective deposition of metallic silver, as the derived thin sections revealed in more detail.

Thin sections from all samples, both implanted and unimplanted, shared silver precipitation sites (i) within nuclei, where metal granules scattered throughout the heterochromatin; and (ii) at the collagen fibril surfaces, along which punctate metal particles adhered with quasi-D-periodical patterns.

Further, distinct silver deposition sites appeared for implanted valve leaflets. On 2-day- and 1-week-implant thin sections, additional sites were represented by (i) the electron-dense material forming both dense bodies and PPM, and (ii) the ECM-derived intravacuolar particles (Fig. 6A,C).

On thin sections of 1-week- to 6-week-implants, PPLs appeared as the major reactive sites because of the greater density and size of silver precipitates (Fig. 6B,D). In addition, PPM-lacking cytoplasms became completely unreactive, except for the nuclear heterochromatin, whereas reactivity was exhibited by PPL-associated floccular material lying at their outer aspect. The same reactivity of PPLs was apparent for PPL-like material spreading into the ECM embedding

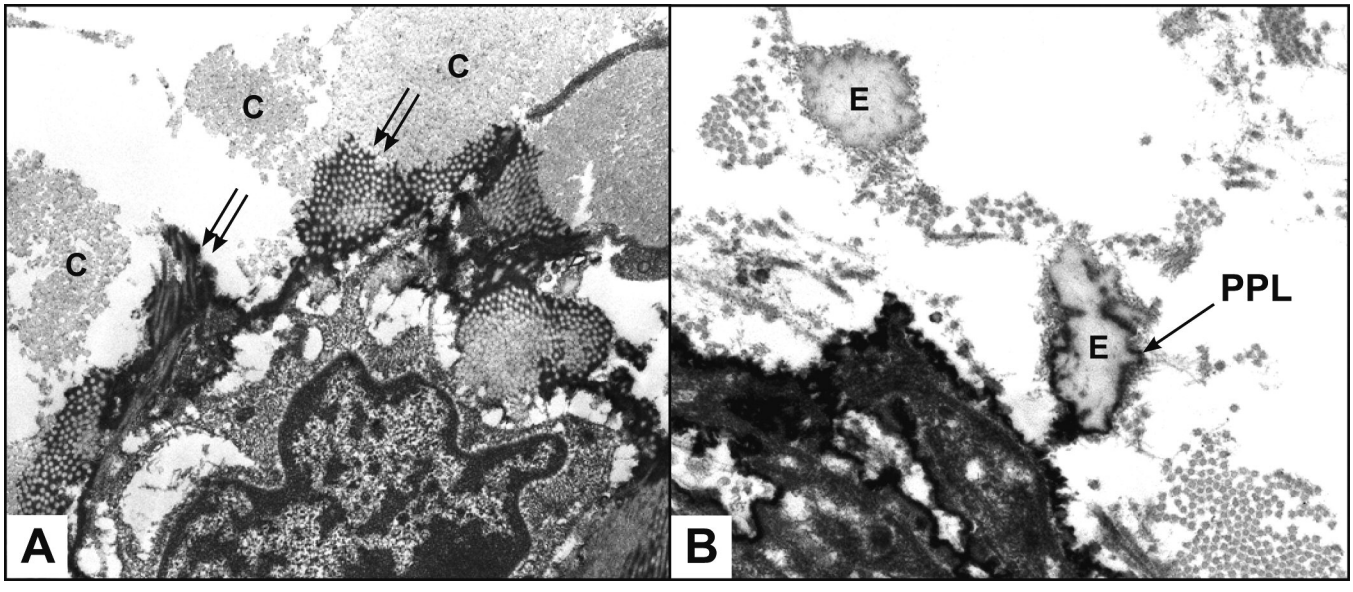

Fig. 5. *Tunica spongiosa* of porcine aortic valve leaflet implanted in rat sub-cutis for 2 weeks. **A.** Presence of PPL and initial spreading of PPL-like material toward the ECM, embedding groups of electronlucent collagen fibrils (double arrows). C: unaffected collagen fibrilis. **B.** PPL-like material enveloping an iuxta-cellular elastin fiber (E). A, x 12,000; B, x 20,000

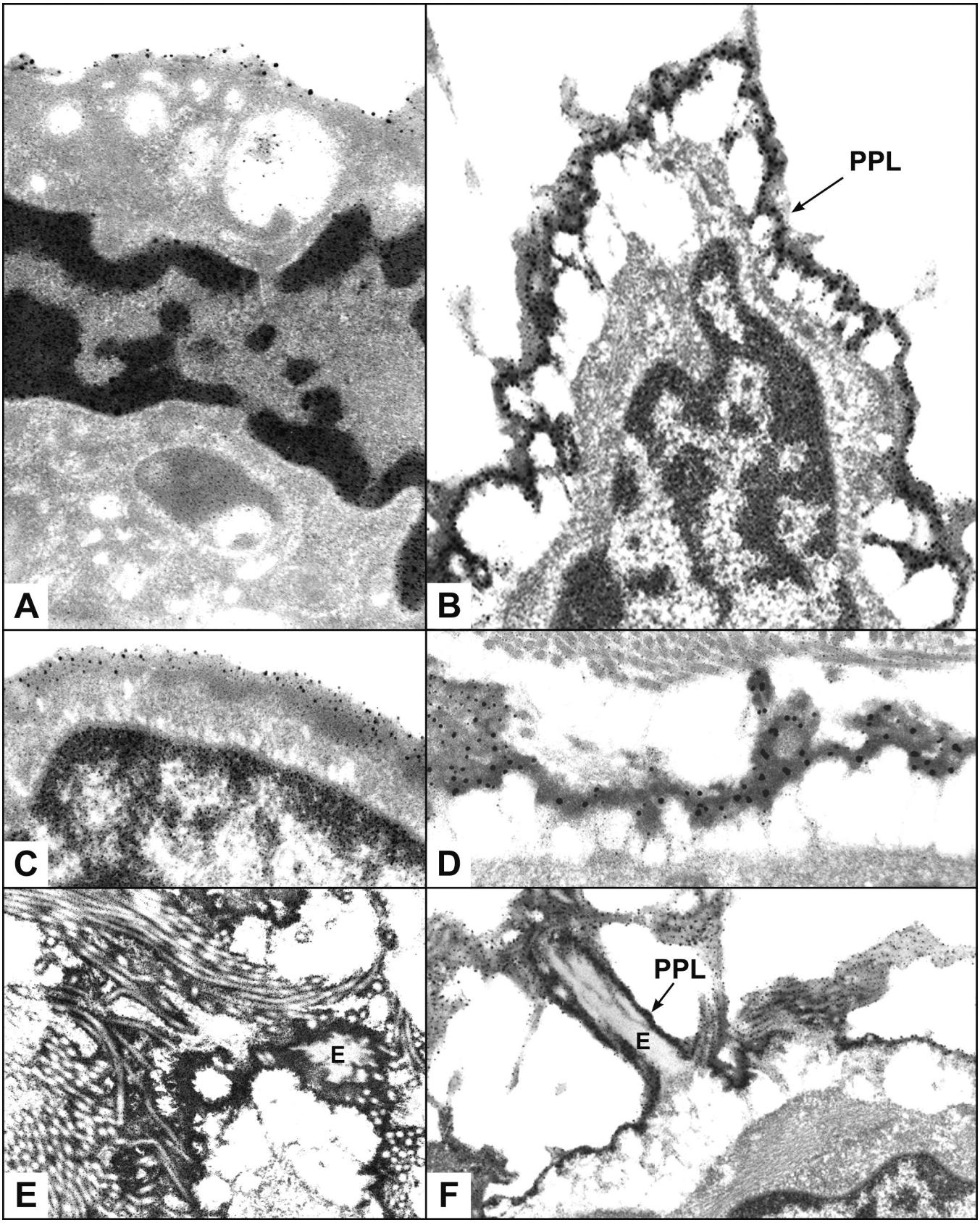

Fig. 6. *Tunica spongiosa* of porcine aortic valve leaflet implanted in rat sub-cutis for 2 days **(A)**, 1 week **(C)**, and 2 weeks **(B, D-F)**. **A-F**. Distribution of metallic silver granules on thin sections derived from von-Kossa-reacted and re-embedded semithin sections. Silver precipitation exhibited by: (i) nuclear heterochromatin (**A-C**); (ii) intravacuolar particles **(A)**; (iii) dense bodies **(A)**; peripheral cytoplasm **(A)**; (iv) PPM **(C)**; (v) PPLs **(B, D-F)**; (vi) and PPL-like material embedding collagen fibrils and elastin fibers (E) **(E,F)**. A, x 39,000; B, x 36,000; C, x 41,000; D, x 42,000; E, x 24,000; F, x 22,000

collagen fibrils and elastin fibers (Fig. 6E,F).

Discussion

The present data add significant information on the tissue changes underlying calcification onset and progression in subdermally implanted aortic valve leaflets and shed light upon the early cell changes and subsequent cascade of degenerative steps preceding the formation of the peculiar mineralization-associated structures called PPLs, as previously described for 6-week implants (Ortolani et al., 2002a,b, 2003).

The spectrometric estimations of Ca indicated that tissue calcification begins within a very short time after implantation and proceeds with implantation time according to a grossly linear pattern, consistently with previous data demonstrating a progressive increase in mineralization to take place in subdermally implanted aortic valves, starting 2 days after implantation, reaching half of the maximum after 3 weeks and the maximum after 8 weeks (Schoen et al., 1985, 1992; Levy et al., 1991). Thus the earliest modifications observed in 2-day implants actually coincided with mineralization onset.

On the basis of previous results (Ortolani et al., 2002a,b) and comparing the observed ultrastructural patterns with the above quantitative results, it appears that: (i) the majority of the estimated Ca will come from deposited amorphous calcium salts, for implants up to 1 week; (ii) additional Ca will come from the needle-shaped apatite crystals accumulating around the cells, for implants older than one week; and (iii) more and more Ca will come from apatite crystals formed at the level of juxtacellular ECM, for implants older than two weeks.

Among the calcium-binding sites ultrastructurally revealed by thin sections after GA-CB-S reactions, PPLs and associated proteinaceous material actually colocalized with the earlier apatite crystal precipitation sites appearing on thin sections after conventional processing.

Since heterogeneous crystallization occurring in biological environments needs the presence of a suitable solid surface acting as a nucleator (Boistelle, 1986), this factor can be represented by the PPL-forming lipidic material, once it is sufficiently condensed and outcrops at the ECM milieu.

If PPL can be identified as an ideal substrate for apatite nucleation, valve stroma can be viewed as an ideal environment for crystal nucleation progression into the ECM, taking into account that rapid apatite proliferation takes place in apatite-enriched serum (Neuman and Neuman, 1958) and a similar medium is represented by rat fluids insudating valve stroma. Consistently, apatite nucleation throughout the ECM will be enhanced by both the spread of PPL-like material outside the cells and the scattering of PPL-derived MV-like bodies, which were also positive to selective metallic silver precipitation.

The additional silver precipitation observed on nuclear heterochromatin and along collagen fibrils in both implants and control samples, seems not to correlate with mineralization processes, as previously discussed for 6-week implants (Ortolani et al., 2003).

The rationale in estimating Cu amounts retained in samples previously subjected to CB-reactions was that this copper-phthalocyanin binds anionic radicals. This parameter is therefore an indirect assay of polyanion content.

The implantation time-dependent changes in Cu retention were significantly different at 0.3M salt CEC conditions *versus* 0.05M. It is well known that 0.3M salt CEC conditions restrict CB-reactivity to sulphated glycosaminoglycans, whereas reactivity also includes non-sulphated glycosaminoglycans, namely hyaluronic acid, as well as non-glycanic polyanions such as nucleotides, at 0.05M (Scott and Dorling, 1965; Scott, 1980).

In 2-day and 1-week implants, reactivity decreased for both CEC conditions, but at a slower rate for 0.05M *versus* 0.3M. Taken together, these results indicate that progressive proteoglycan loss/alteration will occur, as was previously found (Ortolani et al., 2002b). However, the slower Cu decreasing for 0.05M CEC conditions indicates a concurrent increase in polyanionic molecules other than glycosaminoglycans.

This assumption was strengthened by the results concerning the implants older than two weeks, since the amounts of retained Cu tended to plateau for 0.3M CEC conditions, suggesting that loss/degradation of sulphated-glycosaminoglycans had stopped, whereas a trend reversal was apparent for 0.05M CEC conditions, with a possible slight increase taking place between 2 and 4 weeks, and a significant increase between 4 and 6 weeks. Since it is unlikely that additional acidic material may include hyaluronic acid, only non-glycanic anionic substances will be concerned.

Taking into account that GA-CB reactions at 0.05M CEC conditions revealed the first PPLs in 1-week implants and became more and more frequent with implantation times, it is evident that a close relationship exists between the observed increase in copper-linking PPLs and the calculated increase in copper-linking, non-glycanic material, which can actually be regarded as a major PPL component.

Moreover, an endogenous source of PPLs was clearly revealed by the appearance of CB-reactive dense bodies replacing degenerating organules at first, and the subsequent appearance of an additional CB-reactive substance which invaded the entire cytoplasm before moving centrifugally up to stratify into PPLs. Consistently, both dense bodies and PPM were also selective sites for earlier metallic silver precipitation, as observed on thin sections after GA-CB-S reactions.

The derivation of the initial dense bodies was less clear. Concurrent disappearance of cytomembranes and the increase in electron-density of adjacent cytoplasm enabled the clear identification of degenerating mitochondria and nuclear envelopes but other dense bodies resembled remnants of lysosomes or endoplasmic

reticulum cisternae. It is likely that accumulation of lysophospholipids may have generated the first dense bodies, while subsequent, general dissolution of membrane phospholipidic bilayers was a major co-factor in the accumulation of lipid-derived products, contributing to the formation of additional dense bodies as well as diffuse electron-dense material.

On the whole, the acidic nature of accumulating lipidic material will depend on the co-presence of membrane-derived acidic phospholipids, as histochemically shown for 6-week implants (Ortolani et al., 2003), cardiolipin released from inner mitochondrial membranes, and liberation/accumulation of free fatty acids. It must be taken into account that hypoxic/anoxic conditions affect still viable valve cells during pre-implantation treatments, possibly activating phospholipase activities (Abe et al., 1987; Nakano et al., 1990) and/or inducing the accumulation of lactic acid with subsequent hydrolytic effects, as experimentally shown (Barrier et al., 2005).

In addition, the observation of frequent fusion between the above electron-dense inclusions and intracellular vacuoles containing ECM-derived material, which also exhibited positivity to silver staining, suggests that both propensity to calcification and acidity of this PPL-forming material may be also ascribed to the co-presence of products resulting from proteoglycan degradation. In this view, it must be taken into account that calcific properties were reported for modified proteoglycans in physiological calcification (Poole et al., 1982; Arsenault and Ottensmeyer, 1984; Shepard and Mitchell, 1985; Addadi et al., 1987; Takagi et al., 1989; Boskey et al., 1997) and for calcific valve bioprostheses (Jorge-Herrero et al., 1991).

Interestingly, phthalocyanin Alcian Blue staining of human aortic valves affected by age-related dystrophic calcification revealed the presence of membranous material around cell debris, which was assumed to be composed of phospholipids interacting with PGs (Kim and Huang, 1971; Kim, 1976) and is someway reminiscent of PPLs.

Moreover, some functional analogy was assumed to exist (Ortolani et al., 2002a,b, 2003) between PPL-forming lipidic material and the so called "nucleational core complexes", which were found also to include glysosaminoglycan-associated proteins interacting with calcium-acidic-phospholipid-phopsphate complexes and collagens (Wu et al., 1991; Kirsch et al., 1994), suggesting a possible association with PGs and their additional role in promoting calcification.

An unanswered question is what type of upstream cell death will trigger this unusual type of cell degeneration. A wide body of evidence exists to show that calcification is closely related to cell death, with apoptosis as the major candidate in both physiological and pathological calcification (Kim, 1995). However, in vascular pathologies including atherosclerosis, calcific events have been reported to occur via either apoptosis (Proudfoot et al., 2000; Proudfoot and Shanahan, 2001; Jian et al., 2003; Trion and van der Laarse, 2004) or oncosis (Crisby et al., 1997; Wang et al., 1999).

As stressed above, earlier cell death stages likely occur during sample pre-implantation treatment, which is inherent in the calcification model used, because of the presence of nitrogen atmosphere combined with glutaraldehyde-induced toxic effects, while subsequent subdermal implantation will add further critical conditions to already suffering, dying cells. The active cell reactions observed in 2-day-implants, such as the seeming emission and subsequent reabsorption of lamellipodium-like cytoplasm protrusions, were not indicative of apoptosis or oncosis, since there were neither cell body shrinkage, membrane blebbing, or chromatin margination, nor cell swelling, membrane disruption, or cellular content release into the surrounding tissue. However, several alterations, such as the formation of dense bodies, cytoplasm condensation and membrane fading instead of disintegration, could suggest that early apoptosis had started. The absence of more advanced apoptosis-related steps, and their replacement by the degeneration steps as described, can be explained by postulating that apoptosis has been initiated but not completed, owing to the particular sequence of the pre-implantation environment and that existing in rat subcutis.

To highlight the effectiveness of the environment in conditioning tissue modifications, it is worth adding that different effects were also observed to depend on valve leaflet topography. In contrast to the degenerating features exhibited by co-resident, interstitial cells, at the surface of implants up to two weeks, the endothelial cells appeared well preserved, showing features comparable to those in control samples (observation omitted in Result session). This apparently conflicting result can be explained by assuming that, in spite of its low concentration, 0.6% GA can act as an effective fixation agent when interacting with samples directly and promptly. Conversely, a delay in GA entering valve stroma and reaching interstitial cells will enable them to prime early defence mechanisms against increasing hypoxic conditions before they undergo death. This assumption could also explain why more prominent calcification occurs in spongiosa than in fibrosa and ventricularis layers, as observed in the present work in agreement with previous reports (Ferrans et al., 1980; Levy et al., 1983; Schoen et al., 1985; Ortolani et al., 2002a).

Work is in progress to gain further insights into the nature of this type of cell death, the mechanisms involved, and any possible concurrent expression of calcification-associated proteins, as reported (Levy et al., 1980, 1983, 1991; Maranto and Schoen, 1988; Shen et al., 1997; Srivatsa et al., 1997) and suggested by positivity of PPL-associated material to GA-CB-S reactions in the present work and previously (Ortolani et al., 2003).

This study is also going to be extended to human aortic valves affected by calcific stenosis with the aim of

assessing whether the subdermal model is only a convenient procedure to evaluate the calcific propensity of tissues within short times, thanks to its capacity in promoting accelerated mineralization, or actually represents a reliable model for the study in greater detail of the eziopathogenesis and progression steps in pathological calcification.

At present, the results obtained enable better comparison of physiological, pathological and experimental calcification, when applying the same procedures used in this investigation to each of these mineralization processes.

Acknowledgements. This work was supported by grants from the Italian Ministry of the University and Scientific Research (PRIN 2005), the Cassa di Risparmio di Padova e Rovigo Foundation and Regione Friuli Venezia Giulia (L.R.11/2005).

References

Abe K., Kogure K., Yamamoto H., Imazawa M and Miyamoto K. (1987). Mechanism of arachidonic acid liberation during ischemia in gerbil cerebral cortex. J. Neurochem. 48, 503-509.

Addadi L., Moriadian J., Shay E., Maroudas N.G. and Weiner S. (1987). A chemical model for the cooperation of sulfates and carbohydrates in calcite crystal nucleation. Proc. Natl. Acad. Sci. USA 84, 2732-2736.

Anderson H.C. (1983). Calcific diseases: a concept. Arch. Pathol. Lab. Med. 107, 341-348.

Arsenault A.L. and Ottensmeyer F.P. (1984). Visualization of early intramembranous ossification by electron microscopic and spectroscopic imaging. J. Cell Biol. 98, 911-921.

Barrier L., Ingrand S., Piriou A., Touzalin A. and Fauconneau B. (2005). Lactic acidosis stimulates ganglioside and ceramide generation without sphingomyelin hydrolysis in rat cortical astrocytes. Neurosci. Lett. 385, 224-229.

Boistelle R. (1986). The concept of crystal growth from solution. Adv. Nephrol. 15, 173-217.

Bonucci E. (1984). The structural basis of calcification. In: Ultrastructure of the connective tissue matrix. Ruggeri A. and Motta P.M. (eds). Martinus Nijhoff Publishers. Boston. pp 165-191.

Boskey A.L., Bullough P.G., Vigorita V. and Di Carlo E. (1988). Calcium-acidic phospholipid-phosphate complexes in human hydroxyapatite-containing pathologic deposits. Am. J. Pathol. 133, 22-29.

Boskey A.L., Spevak L., Doty S.B. and Rosenberg L. (1997). Effects of bone CS-proteoglycans, DS-decorin, and DS-biglycan on hydroxyapatite formation in a gelatin gel. Calcif. Tissue Int. 61, 298-305.

Chanda J., Kuribayashi R. and Abe T. (1997). Pathogenesis of calcification of native and bioprosthetic valves is different. Circulation 96, 3790-3791

Crisby M., Kallin B., Thyberg J., Zhivotovsky B., Orrenius S., Kostulas V. and Nilsson J. (1997). Cell death in human atherosclerotic plaques involves both oncosis and apoptosis. Atherosclerosis 130, 17-27.

Ferrans V.J., Boyce S.W., Billingham M.E., Jones M., Ishihara T. and Roberts W.C. (1980). Calcific deposits in porcine bioprostheses: Structure and pathogenesis. Am. J. Cardiol. 46, 721-734.

Fishbein M., Levy R.J., Nashef A., Ferrans V.J., Dearden L.C., Goodman A.P. and Carpentier A. (1982). Calcification of cardiac valve bioprostheses: Histologic, ultrastructural, and biochemical studies in a subcutaneous implantation model system. J. Thorac. Cardiovasc. Surg. 83, 602-609.

Jian B., Narula N., Ly Q.Y. Mohler E.R. 3rd and Levy R.J. (2003). Progression of aortic valve stenosis: TGF-beta1 is present in calcified aortic valve cusps and promotes aortic valve interstitial cell calcification via apoptosis. Ann. Thorac. Surg. 75, 457-465.

Jorge-Herrero E., Fernandez P., Gutierrez M. and Casillo-Olivares J.L. (1991). Study of the calcification of bovine pericardium. Analysis of the implication of lipids and proteoglycans. Biomaterials 12, 683-689.

Kim K.M. (1976). Calcification of matrix vesicles in human aortic valve and aortic media. Fed. Proc. 35, 156-162.

Kim K.M. (1995). Apoptosis and calcification. Scanning Microsc. 9, 1137-1178.

Kim K.M. and Huang S. (1971). Ultrastructural study of calcification of human aortic valve. Lab. Invest. 25, 357-366.

Kirsch T., Ishikawa Y., Mwale F. and Wuthier R.E. (1994). Roles of the nucleational core complex and collagens (types II and X) in calcification of growth plate cartilage matrix vesicles. J. Biol. Chem. 269, 20103-20109.

Levy R.J., Zenker J.A. and Lian J.B. (1980). Vitamin K-dependent calcium-binding proteins in aortic valve calcification. J. Clin. Invest. 65, 563-566.

Levy R.J., Schoen F.J., Levy J.T.,, Nelson A.C., Howard S.L. and Oshry L.J. (1983). Biologic determinants of dystrophic calcification and osteocalcin deposition in glutaraldehyde-preserved porcine aortic valve leaflets implanted subcutaneously in rats. Am. J. Pathol. 113, 143-155.

Levy R.J., Schoen F.J., Flowers W.B. and Staelin S.T. (1991). Initiation of mineralization in bioprosthetic heart valves: studies of alkaline phosphatase activity and its inhibition by AlCl3 or FeCl3 preincubations. J. Biomed. Mater. Res. 25, 905-935.

Mako W.J. and Vesely I. (1997). In vivo and in vitro models of calcification in porcine aortic valve cusps. J. Heart Valve Dis. 6, 316-323.

Maranto A.R. and Schoen F.J. (1988). Alkaline phosphatase activity of glutaraldehyde-treated bovine pericardium used in bioprosthetic cardiac valves. Circ. Res. 63, 844-848.

Nakano S., Kogure K., Abe K. And Yae T. (1990). Ischemia-induced alterations in lipid metabolism of the gerbil cerebral cortex: I. Changes in free fatty acid liberation. J. Neurochem. 54, 1911-1916.

Neuman W.F. and Neuman M.W. (1958). The chemical dynamics of bone. University of Chicago Press. Chicago. pp 169-187.

Nimni M.E., Bernick S., Cheung D.T., Ertl D.C., Nishimoto S.K., Paule W.J., Salka C. and Strates B.S. (1988). Biochemical differences between dystrophic calcification of cross-linked collagen implants and mineralization during bone induction. Calcif. Tissue Int. 42, 313-320.

Ortolani F., Petrelli L., Tubaro F., Spina M. and Marchini M. (2002a). Novel ultrastructural features as revealed by phthalocyanin reactions indicate cell priming for calcification in subdermally implanted aortic valves. Connect. Tissue Res. 43, 44-55.

Ortolani F., Tubaro F., Petrelli L., Gandaglia A., Spina M. and Marchini M. (2002b). Specific relation between mineralization and cuprolinic blue uptake as revealed by copper retention in calcified aortic valves

and ultrastructural evidences. Histochem. J. 34, 41-50.

Ortolani F., Petrelli L., Nori S.L., Spina M. and Marchini M. (2003). Malachite green and phthalocyanin-silver reactions reveal acidic phospholipid involvement in calcification of porcine aortic valves in rat subdermal model. Histol. Histopathol. 18, 1131-1140.

Poole A.R., Pidoux I. and Rosenberg L. (1982). Role of proteoglycans in endochondral ossification: immunofluorescent localization of link protein and proteoglycan monomer in bovine fetal epiphyseal growth plate. J. Cell Biol. 92, 249-260.

Proudfoot D. and Shanahan C.M. (2001). Biology of calcification in vascular cells: intima versus media. Herz 26, 245-251.

Proudfoot D., Skepper J.N., Hegyi L., Bennet M.R., Shanahan C.M. and Weissberg P.L. (2000). Apoptosis regulates human vascular calcification in vitro: evidence for initiation of vascular calcification by apoptotic bodies. Circ. Res. 87, 1055-1062.

Scott J.E. (1980). Localization of proteoglycans in tendon by electronmicroscopy. Biochem. J. 187, 887-891.

Scott J.E. and Dorling J. (1965). Differential staining of acid glycosaminoglycans (mucopolysaccharides) by Alcian Blue in salt solutions. Histochemie 5, 221-233.

Shepard N. and Mitchell N. (1985). Ultrastructural modifications of proteoglycans coincident with mineralization in local regions of rat growth plate. J. Bone Joint Surg. 67, 455-463.

Schoen F.J., Levy J.R., Nelson A.C., Bernhard W.F., Nashef A. and Hawley M. (1985). Onset and progression of experimental bioprosthetic heart valve calcification. Lab. Invest. 52, 523-532.

Schoen F.J., Levy R.J. and Piehler H.R. (1992). Pathological considerations in replacement heart valves. Cardiovasc. Pathol. 1, 29-52.

Schoen F.J., Tsao J.W. and Levy R.J. (1986). Calcification of bovine pericardium used in cardiac valve bioprostheses. Implications for the mechanism of bioprosthetic tissue mineralization. Am. J. Pathol. 123, 134-145.

Shen M., Marie P., Farge D., Carpentier S., De Pollak C., Hott M., Chen L., Martinet B. and Carpentier A. (1997). Osteopontin is associated with bioprosthetic heart valve calcification in humans. C.R. Acad. Sci. III 320, 49-57.

Srivatsa S.S., Harrity P.L., Maercklein P.B., Kleppe L., Veinot J., Edwards W.D., Johonson C.M. and Fitzpatrick L.A. (1997). Increased cellular expression of matrix proteins that regulate mineralization is associated with calcification of native human and porcine xenograft bioprosthetic heart valves. J. Clin. Invest. 99, 996-1009.

Takagi M., Sasaki T., Kagami A. and Komiyama K. (1989). Ultrastructural demonstration of increased sulfated proteoglycans and calcium associated with chondrocyte cytoplasmic processes and matrix vesicles in rat growth plate cartilage. J. Histochem. Cytochem. 37, 1025-1033.

Trion A. and van der Laarse A. (2004). Vascular smooth muscle cells and calcification in atherosclerosis. Am. Heart J. 147, 808-814.

Wang A.Y., Bobryshev Y.V., Cherian S.M., Liang H., Inder R.S., Lord R.S., Ashwell K.W. and Farnsworth A.E. (1999). Structural features of cell death in atherosclerotic lesions affecting long-term aortocoronary saphenous vein bypass grafts. J. Submicrosc. Cytol. Pathol. 31, 423-432.

Wu L.N., Genge B.R. and Wuthier R.E. (1991). Association between proteoglycans and matrix vesicles in the extracellular matrix of growth plate cartilage. J. Biol. Chem. 266, 1187-1194.

Accepted September 20, 2006